Degradation of LiTfO/TEGME and LiTfO/DME Electrolytes in Li-O_2 Batteries

Marco Carboni,[1] Andrea Giacomo Marrani,[1,z] Riccardo Spezia,[2,3] and Sergio Brutti [4,5,*,z]

[1] *Dipartimento di Chimica, Università di Roma La Sapienza, 00185 Rome, Italy*
[2] *LAMBE, Univ Evry, CNRS, CEA, Université Paris-Saclay, 91025 Evry, France*
[3] *Sorbonne Universités, UPMC Univ Paris 06, UMR - CNRS 7616, Laboratoire de Chimie Théorique, 75252 Paris, France*
[4] *Dipartimento di Scienze, Università della Basilicata, 85100 Potenza, Italy*
[5] *CNR-ISC, U.O.S. Sapienza, 00185 Rome, Italy*

In this work we discuss the degradation chemistry on carbon-free electrodes of two ether based electrolytes for Li-O_2 batteries, i.e. tetraethylene glycol dimethyl ether (TEGDME) and dimethoxy ethane (DME) with lithium trifluoromethane sulfonate (LiTfO) as salt. To this aim we developed an all-metallic positive electrode by electrodeposition of a gold dendritic film on a nickel foam (Au@Ni). These carbon-free electro-catalytic electrodes have been used to investigate the degradation chemistry of the electrolytes in Li-O_2 cells by eliminating the parallel parasitic reactions due to the commonly used carbon electro-catalysts. In particular the composition and morphological evolutions of the Au@Ni electrodes after discharge and cycling have been characterized ex situ by Raman Spectroscopy, X-ray Photoemission Spectroscopy and Scanning Electron Microscopy. We also couple this experimental study with thermodynamic predictions about the onset degradation of the DME molecule based on density functional theory calculations. In summary in both DME/LiTfO and TEGDME/LiTfO electrolytes, the degradation involves the oxidation of the ether solvent to a mixture of carbonates and carboxylates/formate/oxalate. DME is apparently more strongly degraded compared to TEGDME whereas the LiTfO anion is highly stable. Calculations suggest the key role played by the singlet oxygen molecule as initiator of the degradation path.

 [DOI: 10.1149/2.0331802jes]

Manuscript submitted December 6, 2017; revised manuscript received December 20, 2017. Published January 5, 2018.

Aprotic lithium-oxygen batteries (Li-O_2) are a challenging and promising technology for future reversible energy storage.[1–6] In fact, with a theoretical specific energy of 3305 Wh kg^{-1}, nonaqueous Li-O_2 batteries can be considered a valid alternative to the common fossil fuels for transportation. Thanks to these promising figures, Li-O_2 batteries have been systematically studied in the last ten years[7] and rewarding performance has been achieved.[8–10]

From the fundamental science point of view, recent advancements have been achieved in the comprehension of the basic redox reactions that rules Li-O_2 batteries,[11–16] in the identification of stable lithium salts[9,17,18] and solvents,[8,19,20] or in the understanding the parasitic reactions.[21–26] Nevertheless many important issues must still be tackled in order to develop commercial Li-O_2 cells,[27] in particular concerning the long term chemical/electrochemical stability of the cell.[8,21,23,28]

Amorphous carbon-based materials are widely adopted as positive electrodes in Li-O_2 cells thanks to their large surface areas, good electrical conductivity, cheap costs and their ability to catalyse both the ORR (oxygen reduction reaction) and the OER (oxygen evolution reaction) with small overpotentials.[7,29–32] However, carbonaceous materials are not fully stable in Li-O_2 cells and participate to electrochemical and chemical parasitic reactions upon cycling.[7,33,34] In fact, many authors demonstrated that the degradation of the carbonaceous matrix in Li-O_2 cells likely leads to the formation of carbonates, carboxylates and formates after few electrochemical cycles[7,21,32,35] and the release of CO_2.[34]

Turning to electrolytes, several classes of organic media have been investigated, i.e. carbonates, ethers, glymes, nitriles and sulfoxides.[7,19] Among them, ethereal solvents show a remarkable stability and allow good performance in Li-O_2 cells.[28,36] As an example, dimethoxy ethane (DME),[37] tetraethylene glycol dimethyl ether (TEGDME),[38] triethylene glycol dimethyl ether (triglyme),[39] bis(2-methoxyethyl) ether (diglyme),[39] tri(ethylene glycol)-substituted trimethylsilane (1NM3)[40] or 1,3-dioxolane (DOL)[39] have been used in Li-O_2 cells and afforded prolonged cycling. Nevertheless, also for ether-based electrolytes, several authors proved the accumulation upon cycling in Li-O_2 cells of degradation by-products.[19,21,39]

In two previous studies, we reported the analysis of the evolution of the surface composition upon cycling of carbon positive electrodes in Li-O_2 cells by ex situ X-ray photoemission spectroscopy (XPS) and other techniques. We highlighted the precipitation and removal upon reduction and oxidation of a complex mixture of partially oxidized carbon-containing by-products in two different TEGDME-based electrolytes.[21,35] However, our experimental approach failed to decouple the degradation originated by the oxidation of the ethereal solvent from that due to the oxidation of the carbon electro-catalyst. In fact, the observed mixture of organic/inorganic C-containing by-products formed upon cycling[7] can originate from the degradation of: (a) the organic solvent, (b) the carbon electro-catalyst, (c) the carbon conductor additive, (d) the lithium salt anion (e.g. trifluoromethane sulfonate, TfO, or bis-(trifluoromethane)sulfonamide, TFSI) and/or (e) the interplay between the degradation of the various carbon-containing molecules/substances within the cell.

In the literature only few studies tackled the decoupling of the parasitic reactivity in Li-O_2 cells originated from the electrolyte[41] or from the carbon electrode,[28,42,43] due to the complex interplay between electrode and electrolyte.[7,21,22,44] As an example, evidences of the degradation of DMSO-, DME- and TEGME-based electrolytes with $LiPF_6$ or LiTFSI salts has been provided by Peng et al.[41,45] on gold and TiC electrodes and by Kundu et al.[46] on Ti_4O_7 electrodes using a LiTFSI/TEGDME electrolyte.

Here we illustrate in the literature the degradation chemistry on carbon-free electrodes of two ether-based electrolytes for Li-O_2 batteries, i.e. tetraethylene glycol dimethyl ether (TEGDME) and dimethoxy ethane (DME) both with LiTfO as salt. To this aim gold dendritic electrodes have been developed by us and used to investigate the degradation chemistry of these electrolytes in Li-O_2 cells decoupled from the parallel parasitic chemistry due to the carbon electro-catalysts. As far as we know, this is the first ever reported study of the degradation of these two common electrolytes in Li-O_2 cells on carbon-free

*Electrochemical Society Member.
[z]E-mail: andrea.marrani@uniroma1.it; sergio.brutti@unibas.it

electrodes, thus focusing exclusively on the parasitic chemistry of these solvent/salt solutions.

Gold, as well as the other noble metals, is an electroactive catalyst for ORR and OER reactions, as demonstrated in the literature.[42,47–49] Moreover Au nanostructures can be easily grown electrochemically, or prepared following chemical routes.[47,50–52] Owing to this, gold nanostructures, both self-standing or deposited/grown on macro-porous metal supports can operate as carbon-free electro-catalysts in Li-O_2 cells as demonstrate by other authors.[7,47,53] As mentioned above, Peng et al. observed the accumulation of Li_2CO_3 and HCO_2Li on porous gold electrodes using $LiPF_6$/TEGDME and $LiPF_6$/DME electrolytes by ex situ Fast-Fourier Infrared Spectroscopy (FT-IR).[41] Similarly, Calvo et al. investigated on gold flat microelectrodes the Li-O_2 reaction mechanism and degradations in $LiPF_6$/DMSO, $LiPF_6$/acetonitrile, and $LiBF_4$/acetonitrile electrolytes by using electrochemical quartz crystal microbalance, mass spectrometry, XPS and atomic force microscopy.[33,54,55] Focusing on the electrolyte degradation chemistry, Calvo et al. highlighted the irreversible accumulation of LiF on the gold electrodes as solid by-product in the case of $LiPF_6$-based electrolytes,[33] likely due to the hydrolysis of the hexafluorophosphate anion.

In this work, nanostructured Au films constituted of nano-dendrites have been grown on metallic nickel foams (Au@Ni) through an electrochemical deposition reaction and characterized by X-ray diffraction, X-ray Photoemission Spectroscopy (XPS) and Scanning Electron Microscopy (SEM) and voltammetry. Nickel foams are well-known inert supports in Li-O_2 cells.[56] Electrodes have been recuperated after discharge and cycling and investigated ex situ. The post mortem analysis of the morphology and surface composition of the electrodes has been carried out by ex situ Raman spectroscopy, Scanning Electron Microscopy (SEM) and XPS. It is important to stress that the use of these carbon-free gold electrodes allows highlighting in the C1s XPS region the chemical nature of organic by-products exclusively originated from the degradation of the solvent molecules. As a final point, we also couple this experimental study with thermodynamic predictions of the onset degradation of the DME model molecule based on density functional theory (DFT) calculations, also considering the very recent evidence of the key-role played by the $^1O_2$ chemical species.[57]

Experimental

Positive electrode material synthesis.—The carbon-free positive electrode materials was synthetized by plating a commercial foil of a Nickel foam (MTI Corporation) with gold nano-dendrites by an electrochemical deposition route. The electrodeposition procedure was adapted from Ref. 58 and it is described below in detail.

The pristine Ni foam was cleaned with acetone in an ultrasonic water bath for 15 min, then etched in HCl 6.0 M for 15 min, rinsed with deionized water, soaked in $NiCl_2$ 10^{-4} M for 4 h, and then rinsed with water and sonicated extensively. A three-electrode electrochemical cell was assembled by using the degreased Ni foam as working electrode, a platinum foil as counter electrode and saturated calomel as reference electrode. The electrodeposition of sheet-like Au nanostructures was performed in an aqueous electrolytic solution 10^{-2} M of $HAuCl_4$, 1.25 M of N-methylimdazole and 0.5 M of H_2SO_4. The N-methylimdazole molecule was used as capping agent. The electrodeposition of sheet-like Au nanostructures was obtained applying a constant potential of 0.4 V for 1800 s via an IVIUM Vertex potentiostat. The final gold-plated Ni foam was washed with deionized water and acetone three times to remove all the traces of the electrolyte solution and the possible water-soluble or acetone-soluble electrodeposition by-products accumulated over the working electrode. The final gold-plated Ni foam (i.e. Au@Ni) was punched into discs with a diameter of 10.0 mm.

Cell preparation and post-mortem electrode preparation procedure.—A MTI Corp. stainless steel lithium−air test cell was used for the electrochemical measurements of Li-O_2 batteries. The positive electrode material was in all cases a Au@Ni disk. The negative electrode material was metallic lithium foil cut into disks (Ø = 1.0 cm, thickness 0.5 mm). Two different electrolytes were prepared and tested by dissolving lithium trifluoromethane sulfonate salt ($LiCF_3SO_3$) in DME or TEGDME (Sigma-Aldrich, moisture controlled grade) with a concentration of 1.0 mol/$Kg_{solvent}$ (1 m). Electrolyte was impregnated on a glass-fiber separator (Whatman). The LiTfO salt and the Au@Ni electrodes were dried at 110°C under vacuum for 12 hours before use. The TEGDME and DME solvents were stored in a glove box and dried on regenerated 3 Å molecular sieves (SigmaAldrich) and lithium chips for at least 15 days. Both cells and electrolyte solutions were prepared in an Ar-filled glove box (Iteco Engineering) with moisture concentration below 0.1 ppm.

The electrochemical cells were galvanostatically discharged/charged in static conditions without gas flow by a pre-fixed O_2 overpressure. A static pressure of 1.2 bar above atmosphere was realized within the cell by filling them with O_2 (5.0 N purity) through a valve after assembling. Gaseous O_2 was spilled from a high-pressure cylinder through a stainless steel gas lines equipped with a molecular sieve-filled moisture trap. Electrochemical tests carried out in absence of O_2 was realized by connecting the as assembled cell directly to the electrochemical testing system without pre-filling with oxygen.

Positive electrodes were recuperated post-mortem after cycling from the electrochemical cells in order to carry out morphological and spectroscopic characterizations. The post mortem electrodes were prepared by: (a) de-assembling the cell, (b) soaking in TEGDME or DME, depending on the adopted electrolytic solution to dissolve the traces of the lithium salt, (c) washed in tetrahydrofuran (THF) three times to remove the solvent residues, (d) dried under vacuum for 3 hours at room temperature and (e) stored in an Ar-filled glove box.

Characterization methods.—A MTI Corp. battery cycler was utilized to carry out galvanostatic tests (GC), adopting a constant current of 0.025 mA cm^{-2}. The specific capacity was obtained by normalizing the final capacity to the area of the positive electrode (i.e. 0.785 cm^2).

Linear Sweep Voltammetry tests (LSV) were carried out by using an IVIUM Vertex potentiostat by applying a scan rate of 0.05 mV s^{-1} in order to evaluate the stability windows of the Au@Ni electrode/electrolytes. Two series of experiments were carried out to evaluate the possible occurrence of parasitic redox reactions in the range of 2.0–4.5 V besides the Li-O_2 redox activity:

1) Anodic and cathodic sweep voltammetry tests of Li/electrolyte/Au@Ni cells filled with Ar;
2) Anodic sweep voltammetry tests of Li/electrolyte/Au@Ni cells filled with O_2.

XPS measurements were carried out using a modified Omicron NanoTechnology MXPS system with a monochromatic X-ray source (Omicron XM-1000) and an Omicron EA-127 energy analyzer. The Al Kα (hν = 1486.7 eV) was used as exciting radiation and it was generated operating the anode at 14–15 kV and 10–20 mA. The pass energy for the survey scan was 50 eV, while it was 20 eV for the other photoionization regions. Take-off angles of 11° with respect to the sample surface normal was adopted. All analyses were performed at room temperature, with a pressure of 2 10^{-9} mbar in the chamber during the spectra detection. The C 1s binding energy (BE) of adventitious carbon, obtained for the pristine cathode Ni/Au was used as internal standard reference for the BE scale (accuracy of ±0.05 eV). This signal, composed by four different peaks, was also subtracted to the other C 1s regions of the spectra related to the cycled simples. In order to theoretically reconstruct the XPS spectra a Shirley function was adopted for the secondary electrons background, whereas the elastic peaks have been fit to pseudo-Voigt functions. In particular, position, fwhm and Gaussian-Lorentzian ratio were free to vary within narrow limits. No traces of sample degradation during the extended X-rays irradiation were detected.

X-ray Diffraction (XRD) measurements were carried out by a Phillips Xpert Pro Diffractometer. The morphologies of the samples

were investigated by High Resolution Field Emission Scanning Electron Microscopy instrument (HR-FIELD EMISSION SEM, Auriga Zeiss) and by a Phenom-FEI SEM apparatus.

Raman spectra were carried out by using a micro-Raman spectrophotometer LabRam HR HORIBA Jobin Yvon equipped with a He-Ne (632.8 nm) laser source (20 mW) and a CCD detector. A sealed holder with a sapphire window was adopted in order to protect samples for contact with moisture.

Computational details.—We employed density functional theory (DFT) to calculate molecular properties and to make thermodynamic predictions of the energetics of the C-H bond cleavage reaction of the DME model ether molecule, in order to extend the general degradation model outlined by us in the Ref. 22. Among all the many possible computational approaches adopted previously by many authors to study the degradation of solvents in Li-O_2 environments,[7,16,22,26,59,60] we used the same scheme already exploited and validated by us with respect to highly correlated methods in Ref. 22: the M06-2X functional has been adopted within the 6–311++G∗ basis set.[61] In all calculations we incorporated solvation effects by employing a self-consistent reaction field in continuum solvation model C-PCM.[62] As model solvent we used the of 1,1,2-trichloroethane (present in C-PCM library) which has a dielectric constant very similar to the average value of ethereal solvents. For all ground states of reagents, products and transition states we considered all possible spin states and the reported energy evaluations always refer to the most stable one. Frequency calculations were performed to check that the minima all have real vibrational frequencies and that transition states had only one imaginary frequency. In the case of spin transitions we considered all competing routes. All calculations were carried out by using the Gaussian09 package.[63] The reaction thermodynamics were evaluated in terms of $\Delta_r G^\circ$ at 298.15 K by correcting the variation of the total electronic energy at 0 K between products and reagents, for the vibrational contributions. The $\Delta_r G^\circ$ was calculated as difference between the total energy of products and reagents. The kinetic energy barriers were evaluated in terms of activation energy, E_a, by calculating the energy difference between the reagents and the transition state.

Results and Discussion

The Au@Ni pristine electrode: preliminary characterization.—The synthesized Au@Ni electrodes have been preliminary characterized by SEM, XPS and XRD before testing in Li-O_2 cells as shown in the supplementary information. The Au@Ni electrodes are constituted by an highly crystalline cubic gold phase[64] deposited on the pristine nickel foam (see the figures S1a and S1b). Apparently the electroplating procedure leads to the precipitation of a continuous film that convers the smooth surface of the nickel foam (see the figure S2) and a dense agglomeration of dendrite-like structures grow orthogonal to the nickel structure. Gold dendrites are apparently less than 200 nm thick and are partially fused among them (see the figure S3). Overall, the obtained morphology compares well with that observed by Yang et al. that prepared a similar sample in analogue conditions.[58]

The anodic and cathodic electrochemical stability window both the electrolyte/Au@Ni electrode interfaces in the operating voltage range of a Li-O_2 battery has been evaluated by LSV as shown in the supplementary material (see the figure S3). Negligible catodic currents are detected from the open circuit voltage (OCV, around 3.0 V) to 1.0 V both for the TEGDME and DME based electrolytes. In oxidation two different electrochemical anodic responses are observed in Ar and in O_2. In the Ar-filled cell the anodic stability of both electrolytes over Ni foam/Au is limited to 3.5 V, whereas O_2-filled batteries show a remarkable stability up to 4.6–4.7 V both for TEGDME and for DME. Apparently, the O_2 atmosphere extends the DME and TEGDME-based electrolytes anodic stability window by ∼1 V. It is likely that the formation of a thin passivation layer occurs over the cathode surfaces under oxygen atmosphere, thus shifting the onset voltage of the electrolyte decomposition reaction. A similar behavious has been observed for the bare Ni foam by Liu et al.[56]

Performance of the Au@Ni electrodes in Li-O_2 cells.—Galvanostatic tests have been carried out on Li-O_2 cells assembled with LiTfO/TEGDME and LiTfO/DME as electrolytes. Two different experiments have been carried out: (i) a full cell discharge to a cell voltage of 2.0 V at j = 0.025 mAcm^{-2} and (ii) 5 discharge/charge cycles in a voltage range between 2.0 and 4.1 V with a capacity limitation of 0.1 mAh cm^{-2}, applied both in discharge and charge. The galvanostatic cell voltage profiles are shown in Figure 1.

The Ni foam is unable to catalyse the electrochemical reduction of O_2 to give Li_2O_2,[56] but gold, as well as the other noble metals, is an electroactive catalyst in Li-O_2 cells as demonstrated by many authors[42,47–49] and here shown in the Figures 1a and 1b. The Au@Ni electrodes are able to supply a discharge capacity that approaches 0.4 and 1.0 mAh cm^{-2} for the TEGDME and the DME-based electrolytes, respectively, in the typical voltage range of the O_2/Li_2O_2 redox activity with moderate overvoltages.[7]

The difference in the discharge capacity measured with the two electrolytes may be attributed to the complex interplay between the O_2^- and Li^+ solvation and the Li_2O_2 growth mechanism, i.e. the solution vs. surface mediated paths, that is modulated by the acceptor and donor numbers (DN) of solvents and lithium salt anions.[9,14,16,65–67] In our case, the DN of the TEGDME, DME and the TfO^- anion are 16.6, 20 and 16.9 kcal mol^{-1}.[66,68] Following the model proposed by Burke and co-workers,[66] in the TEGDME/LiTfO electrolyte one may expect an high solvent occupation in the Li^+ solvation shell. On the contrary, the model predicts a high anion occupation of the Li^+ solvation shell in the DME/LiTfO electrolyte. On this basis one may speculate about the possible enhancement of the solution mediated Li_2O_2 growth mechanism in the DME/LiTfO electrolyte, compared to the TEGDME/LiTfO, that may lead to an increase of the overall discharge capacity.[9,66] However, a detailed analysis of this phenomenon is beyond the scope of this article.

It is important to underline that the here shown performance is far from those observed for carbon electrodes.[10,31] However, our goal is not to develop carbon-free application-ready electrode materials for Li-O_2 batteries, but to investigate the electrochemical/chemical stability of the electrolyte solutions on carbon-free electrodes. In this view our Au@Ni positive electrode material is a satisfactory compromise between a reasonable electrochemical response and a model electro-catalytic system for Li-O_2 reaction mechanism studies.

The voltage profiles in discharge/charge cycles of the Au@Ni with the TEGDME-based electrolyte (Figure 1c) show the expected reversible electrochemical response. The discharge plateau in the first discharge occurs at 2.5 V while all the next ones at 2.7 V, thus suggesting a possible increase of the catalytic activity upon cycling. On the contrary, large and increasing overpotentials occur in charge leading to an incomplete reversibility of the processes. In fact, whereas the discharge capacity in all the 5 cycles reached the 0.1 mAhcm^{-2} limitation, the corresponding charge capacity drastically reduces from the 1st to the 5th cycle, reaching a Coulombic efficiency < 60% in the fifth cycle. This different evolution of the overpotentials in the ORR and OER likely originates from an asymmetric variation of the charge transfer resistance of the two processes.

The cells with the DME-based electrolyte show a different behavior. In the discharge/charge cycles (see Figure 1d), the first discharge presents a plateau at 2.7 V while larger overpotentials occur in the following discharges. A similar trend is also observed in the charge profiles, thus leading to an overall capacity fading with a coulombic efficiency between charge and discharge of 70–80% in all cycles. The symmetric increase of the overpotentials upon discharge and charge in the DME-based electrolyte may be attributed to a parallel increase of the overall electrode resistance in both ORR and OER.

The capacity fading upon cycling for both electrolytes may be related to the accumulation of a mixture of reaction products (e.g. LiO_2, Li_2O_2, Li_2O, Li_2CO_3 and possible complex organic by-products) on the surface of the positive electrode upon discharge.[21] Upon charge,

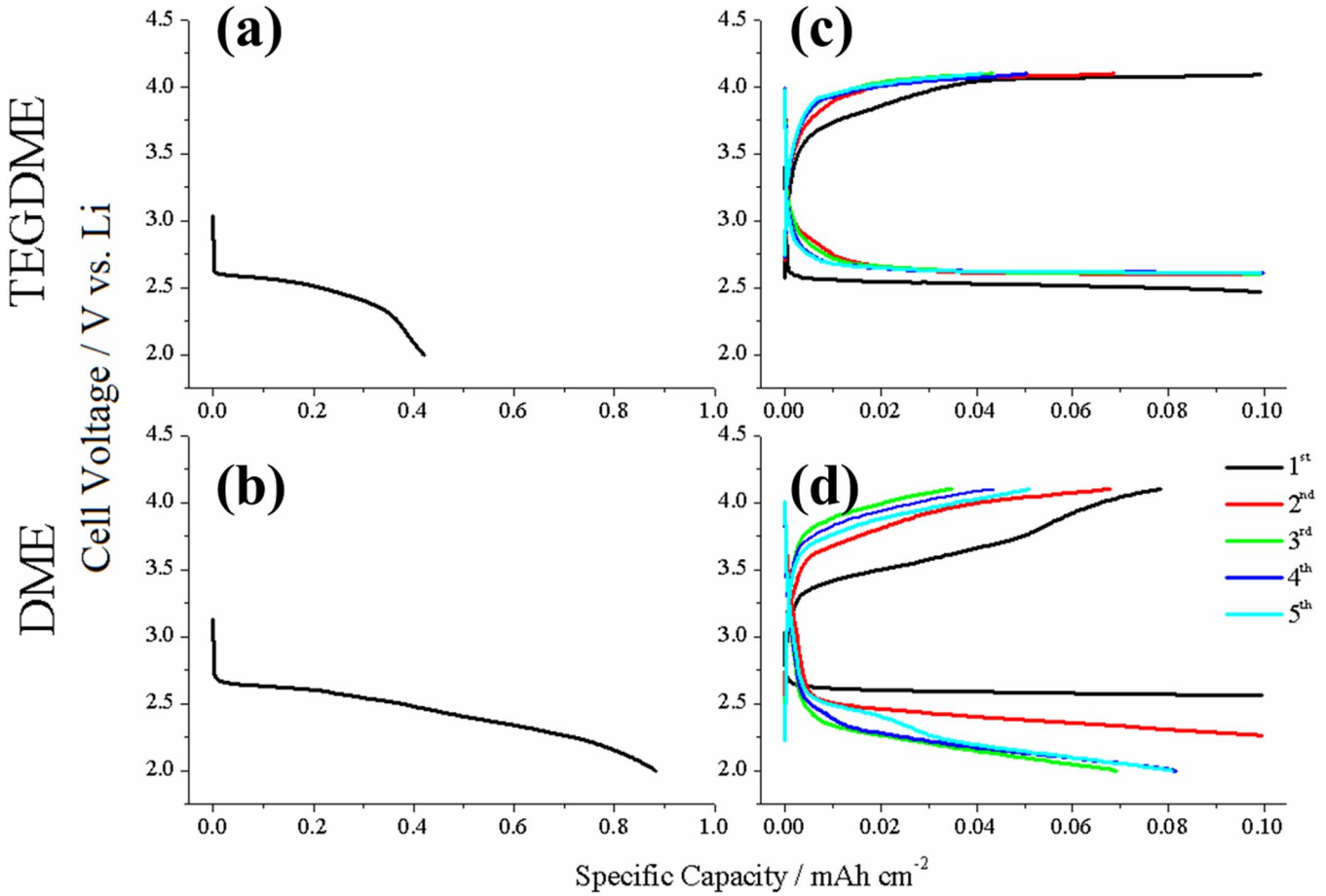

Figure 1. Galvanostatic voltage profiles upon full discharge at 2.0 V for the (a) TEGDME-based and the (b) DME-based electrolytes. Voltage profiles in discharge/charge cycles limited to 0.1 mAh cm^{-2} and between 2.0 and 4.1 V for the (c) TEGDME-based and the (d) DME-based electrolytes.

due to the low anodic voltage cutoff (i.e. 4.1 V vs. Li),[7,21] the removal of the reaction products, or by-products through oxidation to CO_2, is likely incomplete. Therefore, cycle-by-cycle, the electrode surface is slightly passivated, thus leading to an increase of the charge transfer resistance at the interface. On passing one may speculate that the different trends of the ORR and OER overpotentials in the TEGDME and DME electrolytes may originate by possible different the reaction mechanisms for the Li_2O_2 precipitation/dissolution, calling for an inequivalent solvent degradation chemistries.

Post-mortem characterization of Au@Ni electrodes after discharge and cycling.—The reaction products formed after full discharge in Li-O_2 cells in both electrolytes have been identified by ex situ Raman spectroscopy, as shown in Figure 2.

Both Raman spectra highlight the precipitation of Li_2O_2 on the surface of the Au@Ni electrodes recuperated from Li-O_2 cells after discharge to 2.0 V in TEGDME and DME electrolytes, thus confirming the occurrence of the ORR in both cases. Moreover, the possible accumulation of Li_2CO_3 can be highlighted on the electrode discharged in the DME-based electrolyte. This is a clue of the degradation of the DME molecules upon reduction.

The morphology of the Au@Ni electrodes at the end of the discharge at 2.0 V in both electrolyte is shown in the Figure 3 compared to the pristine surface.

The morphology of the surface of the gold electro-catalyst is strongly modified after full discharge at 2.0 V in both electrolytes: dendrites are covered by round shaped particles, partially fused with each other, of approximately 100–200 nm in diameter. These particles are likely constituted by the Li_2O_2 phase identified by Raman spectroscopy.

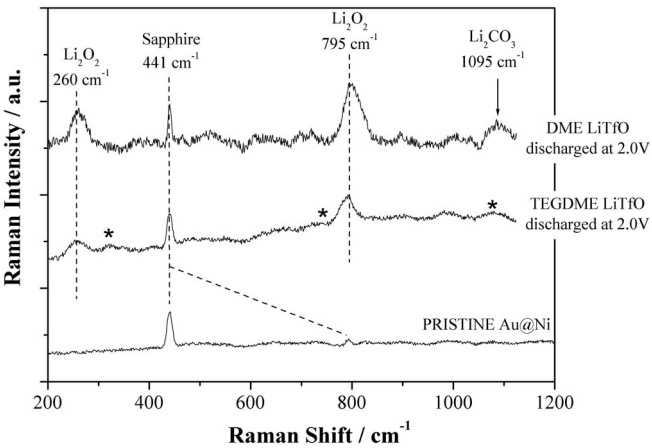

Figure 2. Raman spectra of the Au@Ni electrodes recuperated from Li-O_2 cells after discharge to 2.0 V in TEGDME and DME electrolytes. Broad bands indicated by (*) are possibly due to the LiTfO salt.

After 5 cycles at limited capacity the Au@Ni electrodes show a different surface morphology depending on the used electrolyte as shown in Figure 4.

The SEM micrographs of the Au@Ni electrodes after cycling show a remarkable alteration of the electrode surface morphology both the TEGDME (Fig. 4a) and the DME (Fig. 4b) based electrolytes. In fact, in the case of the TEGDME LiTfO electrolyte the gold dendrites at the end of the 5th charge are apparently clean but the surface is covered

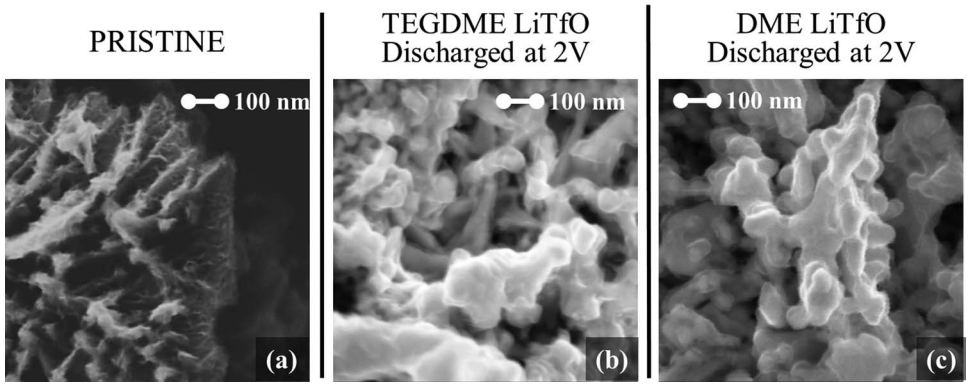

Figure 3. SEM micrographs of the Au@Ni electrodes: (a) pristine electrode; (b) after discharge to 2.0 V in a TEGDME-based electrolyte and (c) after discharge to 2.0 V in a DME-based electrolyte.

by a dispersion of very small particles (bright spots in the Figure 4a). On the other hand, the surface of the Au@Ni electrodes after cycling in the DME LiTfO electrolyte is largely covered by a smooth material that almost covers the gold dendrites (see the Figure 4b).

In both cases, the morphological alteration of the gold dendrites film surface is compatible with the occurrence of parasitic reactions involving the electrolyte degradation and precipitation of insoluble by-products over the positive electrode surface.

In order to analyze the composition evolution of the Au@Ni electrodes upon discharge and cycling in the two different electrolytes, XPS spectra have been recorded for the pristine Au@Ni electrode, after the complete discharge at 2.0 V (D2.0 V) and after 5 galvanostatic cycles between 2.0–4.1 V (D2.0-C4.1 V) both in the TEGDME and DME based electrolytes.

The experimental spectra for C 1s region are shown in Figure 5; assignments and fitting parameters are listed in Table I.

The spectra of Au@Ni pristine electrodes show the expected unavoidable presence of adventitious carbon species. As mentioned in the Experimental section these peaks have been used as internal standard for BE scale referencing, and, assuming that their intensity is constant throughout the different samples, they have been added unaltered to the fitting reconstruction of discharged and cycled electrodes C 1s signals.

In the Au@Ni samples after discharge or cycling in the TEGDME/LiTfO electrolyte, besides the components of the adventitious species, the TEGDME and the TfO^- anion likely chemisorbed onto the electrode, additional lines due to carbonates and carboxylates/formate/oxalate appear at 288.8 and 290.3 eV, respectively. These signals are diagnostic of the occurrence of the degradation of the TEGDME solvent molecules upon discharge and cycling. In particular it is to be noted that the deep discharge to 2.0 V leads to the precipitation of carbonates whereas the cycling leads to the accumulation of a mixture of carbonates and other partially oxidized carbon species.

A similar picture is obtained also for the Au@Ni electrodes discharged and cycled in the DME/LiTfO electrolyte. At the end of the discharge at 2 V, beyond the peak attributable to DME, the presence of a signal at higher binding energy (290.4–290.6 eV) due to carbonates and partially oxidized carbon species, demonstrates the oxidation of the solvent. After cycling, these peaks slightly increase in intensity compared to the adventitious carbon and the TfO^- anion, calling for a significant accumulation of reaction by-products along the 5 cycles. Compared to the TEGDME degradation the accumulation of degradation by-products is apparently larger in the DME-based electrolyte in agreement with the corresponding massive alteration of the electrode reported in the SEM images (see Figs. 4a and 4b). Apparently, our data suggest that the increase of the discharge specific capacity observed in the case of the DME electrolyte occurs at expenses of a larger degradation of the solvent molecules.

The Li 1s regions of the XPS spectra in shown in the supplementary material (see figure S5). The Li 1S spectra of the electrodes discharged and cycled with two LiTfO/TEGDME and LiTfO/DME electrolytes show similar features. As expected, no Li signals can be detected in both the pristine spectra. After discharge, the spectra show broad Li 1s signals, caused by the Li_2O_2 phase identified by Raman spectroscopy and likely convoluted with other features originated from additional lithiated species. In both DME and TEGDME cases, the overall spectral intensities of the Li 1s region are too small and noisy to try any spectral reconstruction and fitting. According to literature,[21] Li_2O, Li_2O_2 and LiTfO can be identified at increasing BE (see also Table I). The possible presence of lithium carbonate Li_2CO_3 should also be taken into account, in agreement with the findings of many research

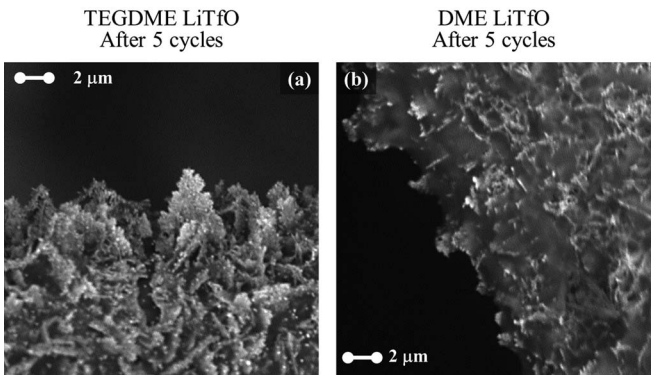

Figure 4. SEM micrographs of the Au@Ni electrodes after 5 galvanostatic cycles in Li-O_2 cells: (a) using a TEGDME-based electrolyte and (b) using a DME-based electrolyte.

Table I. Binding energy positions (BE) and full widths at half maximum (FWHM) values and the assignments of the experimental XPS spectra. FWHM values are only given for the C 1s region.

Peak	BE (eV)/FWHM (eV)	Assignments
C 1s	285.2/1.3-1.5	Adventitious (aliphatic C)
	286.2/1.3	Adventitious (alcohols, ethers)
	288.8/1.3	Adventitious (carboxyl)
	287.3-287.6/1.5	C-O, TEGDME and DME
	288.7-288.9/1.4	-COO-, -COOH-, -C2O4
	290.2-290.4/1.4	-O(C = O)O- carbonate
	293.2-293.4/1.4	$-CF_3$ in $LiCF_3SO_3$
Li 1s	55.4	Li_2O
	56.2	Li_2O_2
	56.8	in $LiCF_3SO_3$

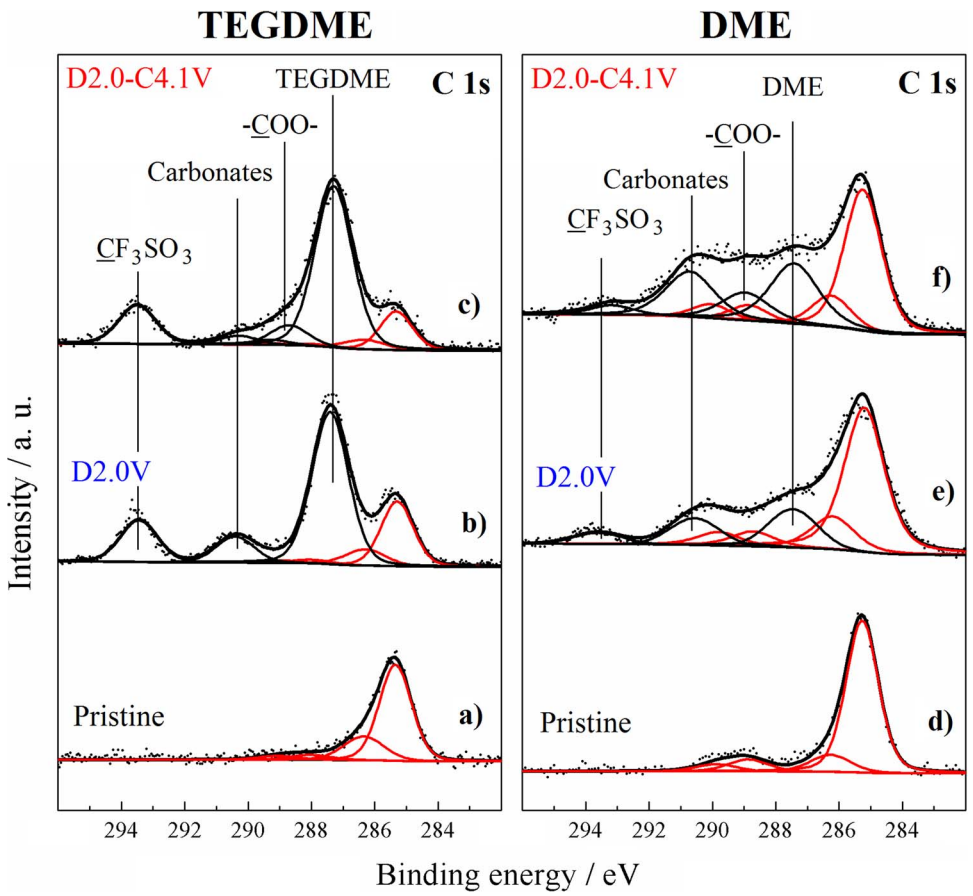

Figure 5. XPS spectra of the C 1s region of the Au@Ni electrodes as prepared (pristine), discharged at 2.0 V (D2.0 V) and after 5 discharge/charge cycles (D2.0 V-C4.1 V) for the TEGDME (a-b-c) and DME (e-f-g) based electrolytes.

groups[7] and our Raman evidence for the DME electrolyte. However the lack of a unique reference value for the Li 1s peak of the lithium carbonate makes its identification sluggish. After 5 discharge/charge cycles, an almost negligible Li 1s signal can be detected in both cases, compatible with the oxidation of deposited lithiated species.

Turning to the other XPS regions, it is interesting to observe the lack in the F 1s XPS region of any feature at about 685 eV possibly attributed to the precipitation of LiF[69] (see the figure S6 in the supplementary material). This degradation by-product has been observed by Marchini et al.[33] in $LiPF_6$/DMSO electrolytes and it is a direct probe of the hydrolysis/degradation of the fluorinated lithium salt initiated by water traces in the electrolyte. In our case, its absence is a direct clue of the stability of the TfO^- anion upon discharge and cycling. This evidence is in agreement with the larger covalency of the C-F bond compared to the P-F bond,[70] and thus less prone to hydrolysis The stability of the triflate anion upon cycling in Li-O_2 cells is also nicely highlighted by the constant position of the peaks in the F 1s and the S 2p XPS regions at 689.5–690 eV and 169.5–170 eV, respectively.[21]

In summary, our XPS results highlights that both TEGDME- and DME-based electrolytes participate to a complex and slightly different degradation chemistry upon discharge and charge. In both cases the degradation involves the solvent molecules whereas the triflate anion is stable. Our findings are in agreement with the literature consensus for carbon-containing positive electrodes about the ether degradation chemistry in Li-O_2 cells.[7,28,59,60,71] Our observations nicely compare with the results by FT-IR reported by Peng et al. on C-free gold electrodes recuperated after cycling using the slightly different $LiPF_6$/TEGME and $LiPF_6$/DME electrolytes.[41] In particular Peng et al. highlighted the accumulation upon cycling of carbonate- and carboxylate-group containing chemical species in both electrolytes and also observed a smaller parasitic reactivity of the TEGDME electrolyte compared to the DME. Apparently our findings confirm their results with a different technique also in the case of the LiTfO/DME and LiTfO/TEGDME electrolytes. One may also recall that the accumulation of carboxylate and carbonate organic by-products originated by the degradation of ether solvents agrees with chemical degradation model outlined by us in a previous publication,[22] based on computational thermodynamic predictions.

In the case of the degradation of the TEGDME-LiTfO electrolyte a comparison with our previous results already published for carbonaceous electrodes is straightforward.[21] Apparently two relevant differences can be highlighted in the evolution of the electrode surface composition in the C 1s region of the XPS spectra:

1. The strong reduction of the magnitude of the carbonate component (relative to the adventitious species) at 290–290.5 eV at the end of discharge at 2 V, on the Au@Ni electrodes compared to the carbon electrode;
2. The absence of relevant alterations of the "defective graphitic carbon" components at about 285–285.5 eV on the Au@Ni electrodes compared to the carbon electrode both upon discharge and charge.

One may suggest that both these differences are clues of an additional degradation chemistry that directly involve the carbon electrocatalyst. This speculation agrees with the alteration of the carbon electro-catalyst nanoparticle morphology observed by us after cycling in Ref. 21,35.

The onset degradation reaction of the DME molecule in Li-O_2 cells.—As already mentioned the reaction products observed by XPS for both DME and TEGDME electrolytes (see the Figure 5) nicely

Table II. Standard Gibbs energy of reaction at 298.15 K of various C-H cleavage reactions for the DME molecule in the Li-O_2 environment.

		Stoichiometry	$\Delta_rG^\circ_{298K}$ (±4) kJ mol^{-1}
Homolytic C-H cleavage	R1	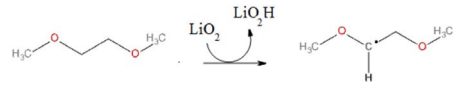	122
	R2	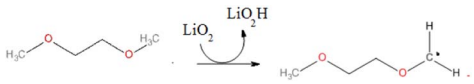	129
	R3	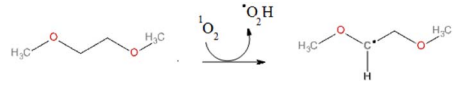	33
	R4	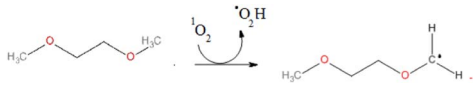	40
Heterolytic C-H cleavage	R5	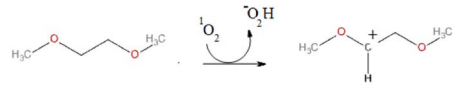	122
	R6	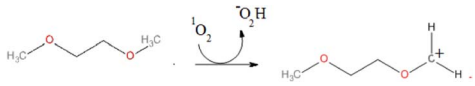	128

match with the chemical reaction model developed by us for the degradation of DME in Ref. 22 based on DFT thermodynamic predictions and with the previous one proposed by Nazar et al.[8] We predicted a complex degradation mechanism driven by the extremely favorable thermodynamics of the formation of formates/acetates/carbonates and anhydrides through the chemical oxidation of the DME molecules by molecular oxygen and superoxide anion. Our model assumed as onset reaction the homolytic H-abstraction from the ether molecule due to a nucleophilic attack from superoxide anions. In the Ref. 22 our choice was made in consideration of the general literature consensus.[7,60,71] In fact, although the C-H bond cleavage can follow different reaction paths (i.e. oxidative instability, surface mediated decompositions or nucleophilic attacks from the peroxide anion on acidic sites on the target molecule)[20,72,73] in the ether-based Li-O_2 cells the nucleophilic attack by the superoxide anion is commonly recognized as the most detrimental, being LiO_2 the first intermediate discharge products identified in the electrochemical reduction of molecular oxygen.[7,15,20,53,71–73]

Very recently the formation of singlet oxygen molecules upon discharge and charge in Li-O_2 cells has been proven experimentally[57,74] and has been put in direct correlation with the parasitic reactivity upon cycling. In the view of this remarkable evidence, it is important to evaluate the reaction thermodynamics and the kinetic energy barriers of the onset reaction of degradation paths involving this additional highly-reactive molecule. Here we illustrate preliminary computational data concerning the onset reaction for the model DME molecule with the aim to update our general degradation scheme proposed in Ref. 22.

In the Table II the energetic predictions obtained by DFT calculations for the Δ_rG° at 298 K of the computed C-H bond cleavage reactions on the DME molecule are summarized.

Having in mind the possible competition between superoxide and singlet oxygen molecules, the C-H bond cleavage may occur in a Li-O_2 environment by:

a. homolytic path initiated by the lithium superoxide, i.e. LiO_2, (reactions R1 and R2) or by the singlet oxygen molecule, i.e. $^1O_2$, (reactions R3 and R4);
b. heterolytic path initiated by the singlet oxygen molecule, i.e. $^1O_2$, (reactions R5 and R6) or from the

Our calculations suggest a positive Gibbs energy of reaction at 298 K for all the computed reactions. However, the nucleophilic attack by the singlet oxygen molecule toward the slightly acidic C-H bonds vicinal to the ethereal oxygen (reactions R3 and R4) show a much smaller Δ_rG° compared to all the other considered processes. The equilibrium constants for the nucleophilic attacks from the singlet oxygen molecule are $\sim 10^{-6}$ and $\sim 2 \bullet 10^{-7}$ for reactions R3 and R4, respectively: these two values are more than 10^{15} larger compared to all thermodynamic constants for the other reactions.

From the kinetic point of view Bryantsev at al.[60] observed a phenomenological correlation between the predicted activation energy, E_a, for the cleavage of the C-H bonds in a wide class of solvents and their experimental chemical stability against KO_2. The kinetic energy barrier, i.e. E_a, is the difference in the total energy between the predicted transition state and the reagents or a reaction and it is by definition positive and larger in comparison to the corresponding overall Δ_rG. Bryantsev highlighted that only solvents with a $E_a > 100 \pm 8$ kJ mol^{-1} are stable in KO_2 environments.

In this consideration, reactions R1, R2, R5 and R6 in the Table II are expected to be kinetically inactive, being their corresponding Gibbs energy of reaction >100 kJ mol^{-1}. Turning to the other two processes, our calculations predicts for reactions R3 and R4 activation energies E_a of 111 ± 4 and 102 ± 4 kJ mol^{-1}, respectively. Thus the activation barrier of the nucleophilic attack toward the slightly acidic C-H bond of the DME from the $^1O_2$ is compatible with the phenomenological threshold suggested by Bryantsev. It is interesting to observe that the hydrogen extraction on the methoxy-carbon (R4) is kinetically more favoured, and thus faster, compared to the homolytic C-H cleavage on the ethoxy-carbon (R3). Although highly speculative and qualitative, one may put this prediction in correlation with the larger degradation chemistry observed experimentally for DME compared to TEGDME (see above). In fact, the ratio between hydrogen atoms bonded to methoxy-carbons and ethoxy-carbons is 1 and 0.25 for the DME and TEGDME molecules, respectively.

In summary, our calculations provide a thermodynamic confirmation that the singlet oxygen molecule, unavoidably released as transient species in the Li-O_2 cells, can play a key role in the cleavage of the slightly acidic C-H bonds in the model ether DME molecule, being the competitive onset reactions initiated by the LiO_2 molecule kinetically inactive. Overall, our calculations suggest that the C-H bond cleavage likely leads to the formation of radical molecules. This prediction updates and strengthen the general DME degradation reaction schemes suggested by us in the Ref. 22 that identifies dimethyl oxalate, methyl formate, 1-formate methyl acetate, methoxy ethanoic methanoic anhydride, and ethylene glycol diformate as final degradation products. On passing it is interesting to underline that the formation of these products is in nice agreement with the here discussed XPS results.

Further computational analyses of the degradation chemistry of other ethers, such as TEGDME, or different solvents, e.g. DMSO or ionic liquids, are needed to confirm the detrimental role of the singlet oxygen molecule and also to understand the difference in mitigated reactivity of TEGDME compared to the DME solvent.

Conclusions

In this work, we studied the chemical instability upon galvanostatic cycling of two common aprotic electrolytes in Li-O_2 battery: i.e. tetraethylene glycol dimethyl ether (TEGDME) and dimethoxy ethane (DME) both with LiTfO as salt. To this aim nanostructured Au films constituted of nano-dendrites have been grown on metallic nickel foams (Au@Ni) through an electrochemical deposition reaction. This material has been used as self-standing positive electrode in Li-O_2 cells. We performed ex situ Raman, X-ray photoemission spectroscopy and scanning electron microscopy analyses of post mortem electrodes recuperated after operation in cell, in order to highlight the accumulation of oxidized carbon species (i.e. carbonates, carboxylates, formates) over the electrode surfaces. Our experimental approach allowed us to unequivocally highlight the degradation of both TEGDME or DME in the Li-O_2 environment without the parallel reactivity of the carbon electro-catalyst. Our multi-technique results provided for the first time detailed insights about the degradation of these two electrolyte formulations on C-free electrodes and confirmed the literature consensus obtained on carbon-containing electrodes. We also coupled our experimental analysis with the thermodynamics predictions of the onset reaction of the degradation route of the model DME molecule. Our calculations based on the DFT confirmed the key-role played by the $^1O_2$ molecule in the activation of the parasitic chemistry and update our general degradation scheme for the DME molecule.

Acknowledgments

M.C. acknowledges the University of Basilicata for the hospitality during their research stages. A.G.M. thanks the University of Rome "La Sapienza" for financial support through the Ateneo Project 2015 (C26A152T5M). S.B. thanks the University of Basilicata for the funding through the RIL 2015 grant.

ORCID

Sergio Brutti https://orcid.org/0000-0001-8853-9710

References

1. P. G. Bruce, S. Freunberger, L. J. Hardwick, and J. -M. Tarascon, *Nat. Mater.*, **11**, 19 (2011).
2. L. Grande et al., *Adv. Mater.*, **27**, 784 (2015).
3. B. Scrosati, *Nature*, **473**, 448 (2011).
4. B. Scrosati and J. Garche, *J. Power Sources*, **195**, 2419 (2010).
5. J. C. Bachman et al., *Chem. Rev.*, **116**, 140 (2016).
6. D. Larcher and J. -M. Tarascon, *Nat. Chem.*, **7**, 19 (2014).
7. P. G. Imanishi, N. Luntz, and A. Bruce, *The Lithium Air Battery: Fundamentals*, Springer, New York (USA), (2014).
8. B. Adams et al., *Adv. Energy Mater.*, **5**, 1 (2015).
9. L. Johnson et al., *Nat. Chem.*, **6**, 1091 (2014).
10. G. A. Elia and J. Hassoun, *Sci. Rep.*, **5**, 12307 (2015).
11. Y. Lu and Y. Shao-Horn, *J. Phys. Chem. Lett.*, **4**, 1 (2013).
12. F. S. Gittleson et al., *ChemElectroChem*, **2**, 1446 (2015).
13. R. Black et al., *Angew. Chemie - Int. Ed.*, **52**, 392 (2013).
14. X. Gao, Y. Chen, L. Johnson, and P. G. Bruce, *Nat. Mater.*, **15**, 882 (2016).
15. Z. Peng, Y. Chen, P. G. Bruce, and Y. Xu, *Angew. Chemie - Int. Ed.*, **54**, 8165 (2015).
16. D. G. Kwabi et al., *Angew. Chemie Int. Ed.*, **55**, 3129 (2016).
17. G. A. Elia, J. -B. Park, Y. -K. Sun, B. Scrosati, and J. Hassoun, *ChemElectroChem*, **1**, 47 (2014).
18. D. G. Kwabi et al., *J. Phys. Chem. Lett.*, **7**, 1204 (2016).
19. D. Sharon, D. Hirshberg, M. Afri, A. A. Frimer, and D. Aurbach, *Chem. Commun.*, **53**, 3269 (2017).
20. V. S. Bryantsev et al., *J. Electrochem. Soc.*, **160**, A160 (2012).
21. M. Carboni, S. Brutti, and A. G. Marrani, *ACS Appl. Mater. Interfaces*, **7**, 21751 (2015).
22. M. Carboni, A. G. Marrani, R. Spezia, and S. Brutti, *Chem. - A Eur. J.*, **22**, 17188 (2016).
23. B. D. McCloskey et al., *J. Phys. Chem. Lett.*, **3**, 3043 (2012).
24. B. . McCloskey et al., *J. Phys. Chem. Lett.*, **3**, 997 (2012).
25. J. M. García, H. W. Horn, and J. E. Rice, *J. Phys. Chem. Lett.*, **6**, 1795 (2015).
26. R. S. Assary, K. C. Lau, K. Amine, Y. K. Sun, and L. A. Curtiss, *J. Phys. Chem. C*, **117**, 8041 (2013).
27. D. Sharon et al., *J. Solid State Electrochem.*, **21**, 1861 (2017).
28. S. A. Freunberger et al., *Angew. Chemie - Int. Ed.*, **50**, 8609 (2011).
29. A. Rinaldi, O. Wijaya, and H. Hoster, *ChemElectroChem*, **3**, 1944 (2016).
30. J. Højberg et al., *ACS Appl. Mater. Interfaces*, **7**, 4039 (2015).
31. A. I. Belova, D. G. Kwabi, L. V. Yashina, Y. Shao-Horn, and D. M. Itkis, *J. Phys. Chem. C*, **121**, 1569 (2017).
32. D. Hirshberg, O. Yariv, G. Gershinsky, E. Zinigrad, and D. Aurbach, *J. Electrochem. Soc.*, **162**, A7001 (2015).
33. F. Marchini et al., *Langmuir*, **31**, 9236 (2015).
34. L. McCloskey, B. Valery, A. Luntz, A. Gowda, S. Wallraff, G. Garcia, J. Mori, and T. Krupp, *J. Phys. Chem. Lett.*, **4**, 2989 (2013).
35. D. Giacco, M. Carboni, S. Brutti, and A. G. Marrani, *ACS Appl. Mater. Interfaces*, **9**, 31710 (2017).
36. P. Du et al., *Phys. Chem. Chem. Phys.*, **15**, 5572 (2013).
37. I. M. Markus, G. Jones, and J. M. García, *J. Phys. Chem. C*, **120**, 5949 (2016).
38. M. Christy et al., *J. Power Sources*, **342**, 825 (2017).
39. D. Sharon et al., *J. Phys. Chem. Lett.*, **4**, 127 (2013).
40. P. Du et al., *Phys. Chem. Chem. Phys.*, **15**, 5572 (2013).
41. Z. Peng, S. A. Freunberger, Y. Chen, and P. G. Bruce, *Science*, **337**, 563 (2012).
42. C. Liu and S. Ye, *J. Phys. Chem. C*, **120**, 25246 (2016).
43. M. Song et al., *J. Solid State Electrochem.*, **17**, 2061 (2013).
44. D. Zhu et al., *J. Solid State Electrochem.*, **17**, 2865 (2013).
45. M. M. Ottakam Thotiyl et al., *Nat. Mater.*, **12**, 1050 (2013).
46. D. Kundu, R. Black, E. Amstorp Berg, and L. F. Nazar, *Energy Environ. Sci.*, **8**, 1049 (2015).
47. H. Yang, J. Xia, L. Bromberg, N. Dimitrov, and M. S. Whittingham, *J. Solid State Electrochem.*, **21**, 463 (2017).
48. Y. -C. Lu et al., *J. Am. Chem. Soc.*, **132**, 12170 (2010).
49. J. Zhang et al., *Electrochim. Acta*, **151**, 415 (2015).
50. L. An, Y. Wang, Q. Tian, and S. Yang, *Materials (Basel)*, **10**, 1372 (2017).
51. T. Wang, Y. Jiao, Q. Chai, and X. Yu, *Nano Life*, **5**, 1542007 (2015).
52. W. Li, X. Zhao, Z. Yi, A. M. Glushenkov, and L. Kong, *Anal. Chim. Acta*, **984**, 19 (2017).
53. N. Mahne, O. Fontaine, M. M. Ottakam Thotiyl, M. Wilkening, and S. A. Freunberger, *Chem. Sci.*, **8**, 6716 (2017).
54. M. del Pozo, W. R. Torres, S. E. Herrera, and E. J. Calvo, *ChemElectroChem*, **3**, 1537 (2016).
55. W. R. Torres, L. Cantoni, A. Y. Tesio, M. Del Pozo, and E. J. Calvo, *J. Electroanalytical Chem.*, **765**, 45 (2016).
56. X. Liu, D. Wang, and S. Shi, *Electrochim. Acta*, **87**, 865 (2013).
57. N. Mahne et al., *Nat. Energy*, **2**, 17036 (2017).
58. F. Yang, K. Cheng, G. Wang, and D. Cao, *Electrochim. Acta*, **159**, 111 (2015).
59. V. S. Bryantsev and F. Faglioni, *J. Phys. Chem. A*, **116**, 7128 (2012).
60. V. S. Bryantsev et al., *J. Phys. Chem. A*, **115**, 12399 (2011).
61. Y. Zhao and D. G. Truhlar, *Theor. Chem. Acc.*, **120**, 215 (2008).
62. M. Cossi, N. Rega, G. Scalmani, and V. Barone, *J. Comput. Chem.*, **24**, 669 (2003).
63. M. Frisch, *Gaussian 09*, p. 2, Gaussian, Inc., Wallingford, CT, (2009).
64. J. Donohue, *The structure of elements*, Wiley, New York (US), (1974).
65. F. S. Gittleson et al., *Phys. Chem. Chem. Phys.*, **16**, 3230 (2014).
66. C. M. Burke, V. Pande, A. Khetan, V. Viswanathan, and B. D. McCloskey, *Proc. Natl. Acad. Sci.*, **112**, 9293 (2015).
67. C. O. Laoire, S. Mukerjee, K. M. Abraham, E. J. Plichta, and M. A. Hendrickson, *J. Phys. Chem. C*, **114**, 9178 (2010).
68. W. Linert et al., *J. Chem. Soc., Dalt. Trans.*, **9**, 3181 (1993).
69. G. E. Murch and R. J. Thorn, *J. Phys. Chem. Solids*, **41**, 785 (1980).
70. M. Carboni, R. Spezia, and S. Brutti, *J. Phys. Chem. C*, **118**, 24221 (2014).
71. B. Luntz, A. McCloskey, A. C. Luntz, and B. D. McCloskey, *Chem. Rev.*, **114**, 11721 (2014).
72. N. Kumar, M. D. Radin, B. C. Wood, T. Ogitsu, and D. J. Siegel, *J. Phys. Chem. C*, **119**, 9050 (2015).
73. A. Khetan, A. Luntz, and V. Viswanathan, *J. Phys. Chem. Lett.*, **6**, 1254 (2015).
74. J. Wandt, P. Jakes, J. Granwehr, H. A. Gasteiger, and R. -A. Eichel, *Angew. Chemie*, **128**, 7006 (2016).